Motor Temperature Monitoring Based on Impedance Estimation at PWM Frequencies

Nikola Popov[1], Slobodan N. Vukosavic[1], *Senior Member, IEEE*, Emil Levi[2], *Fellow, IEEE*

[1]University of Belgrade, Dept. of Electrical Engineering, 11000 Belgrade, Serbia (e-mail: boban@ieee.org)
[2]Liverpool John Moores University, School of Engineering, Liverpool L3 3AF, UK (e-mail: e.levi@ljmu.ac.uk)

***Abstract*–This paper proposes a non-invasive temperature measurement technique of indirect type, applicable in the permanent magnet synchronous motor (PMSM) drives. The motor temperature is required for protection and monitoring purposes, as well as for updating temperature dependent control parameters. Direct measurement with dedicated sensors requires peripherals and cabling; hence it is quite involved and often avoided. Temperature estimation based on test signal injection contributes to torque ripple and often relies on other motor parameters. A solution is proposed here, which makes the use of intrinsic PWM excitation and which does not make use of electrical or thermal parameters of the considered PMSM. The temperature of the stator winding is estimated from the motor input impedance $Z_{IN}(\omega)$ calculated over the range of frequencies starting at and going well beyond f_{PWM}. The paper includes analytical considerations, implementation details and experimental verification obtained with a 4.5 kW PMSM used in battery-supplied propulsion systems.**

***Index Terms*–Permanent magnet synchronous machines, PWM inverters, Temperature monitoring.**

I. Introduction

PMSMs are widely used due to their favourable efficiency and large torque-to-inertia ratio. Most PMSMs have a three-phase stator winding supplied from a PWM controlled three-phase voltage source inverter. Getting the most out of the given copper and iron is a commonly adopted rule in designing and using electrical machines. If overloaded, PMSM drives are exposed to elevated temperatures that may damage the winding insulation [1], de-flux the magnets [2], cause accelerated aging, and affect the performance.

In order to maximize the torque and power output without exceeding the temperature limit, it is necessary to track the actual motor temperature. Direct measurement by means of a dedicated sensor provides only the local temperature at the sensor mounting spot. A number of distributed sensors is required to obtain the proper thermal status of the motor and eliminate delays caused by the thermal inertia. This in turn contributes to a great deal of cabling and reduces the system reliability [3]. For this reason, sensorless estimation of the motor temperature is preferred with the aim of achieving thermal monitoring, over-temperature protection and updating of temperature sensitive parameters.

The average temperature of the stator windings can be obtained by estimating the stator resistance R_S [4], [5], which changes with the temperature. The value of R_S can be calculated from the voltage drop $R_S i_S$, derived from fundamental components of U_S and I_S [6], but this requires a thorough knowledge of the remaining PMSM parameters and fails in all cases where $R_S i_S << U_n$, which is the case in all large power drives. The alternative approach is the test signal injection [7] which operates at test frequencies decoupled from the fundamental, thus eliminating the sensitivity of the R_S estimate to the PMSM operating regime or to variation of the remaining parameters. Elevated test frequencies secure decoupling of the estimator from fundamental voltages and currents, but they make the R_S estimate more sensitive to the winding capacitances, parasitic phenomena [8], and delays in PWM and A/D lines. On the other hand, test signals at lower frequencies disturb the fundamental behaviour of PMSM drives by introducing additional losses and torque ripple. Several test signal methods are compared in [5] and an optimized current injection method is proposed, conceived to reduce the test signal induced power losses and to minimize the impact of the intermittent pulsing on the motor fundamental behaviour. With amplitude of injected current corresponding to the rated continuous current, the motor temperature is estimated with a precision better than 10°C.

The power losses and disturbances introduced by intermittent test signal injection may not be acceptable in a number of applications of PMSM drives. At the same time, all the methods based on detecting the $R_S i_S$ voltage drop fail to detect the winding temperature of very large motors, where the relative value of $R_S I_n$ falls well below 1% [5]. With $R_S I_n$ = 1% and 12-bit resolution of the voltage reading, the resolution of R_S-based temperature reading is roughly 10° C.

In this paper, a novel sensorless temperature estimator is proposed, based on detecting the temperature-related changes of the PMSM input impedance. It does not require test signal injection and it makes no use of the remaining electrical or thermal parameters of the motor. At the same time, proposed method is suitable even for very large PMSM drives with very low values of R_S. Instead of test signals, the method uses the PWM voltage pulses as an intrinsic input disturbance available from all three-phase inverters. The same approach has been advantageously used in estimating the rotor position in shaft-sensorless drives [9-13].

In Section II, PMSM response to high frequency excitation is analyzed and discussed. Temperature related changes of the input impedance are found to be a viable means for sensorless temperature estimation even with PMSM drives with very low R_S. Proposed estimator is introduced and explained in Section III, along with some key implementation details.

Experimental results, obtained with a 4.5 kW PMSM drive, are given in Section IV, while Section V summarizes conclusions and discusses potential applications.

II. Temperature Changes in PMSM Impedance

A. Preliminary Considerations

Trains of PWM voltage pulses $u_S(t)$ across the PMSM stator terminals produce an approximately triangular-shaped current ripple in the stator current $i_S(t)$. The ratio $U_S(j\omega)/I_S(j\omega)$ represents the input impedance $Z_{IN}(j\omega)$ at the given excitation frequency ω. The values of $U_S(j\omega)$ and $I_S(j\omega)$ can be obtained by applying FFT on sample trains of $u_S(t)$ and $i_S(t)$. With PWM voltages used as intrinsic test signal, values of $Z_{IN}(j\omega)$ can be obtained in an interval of frequencies that starts with $\omega_{PWM}=2\pi f_{PWM}$ and goes well beyond f_{PWM}, covering higher harmonics of the PWM pulse train.

The electromotive force $e(t)$ of a PMSM does not have spectral components at frequencies $f>f_{PWM}$. Neglecting the iron losses and the winding capacitance, the equivalent circuit of the motor reduces to series connection of the stator resistance $R_S(\omega)$ and the stator inductance $L_S(\omega)$ (Fig. 1).

The winding temperature θ_W affects the stator resistance $R_S(\omega)$ by changing the specific resistance of copper $\rho = 1/\sigma$. Therefore, derivation of $R_S(\omega)$ is a viable means for the temperature estimation. It should be noted that $R_S(\omega)$ has a considerably larger value at elevated frequencies due to skin effect [14], [15]. For this reason, detecting temperature changes in $R_S(\omega)$ values obtained at frequencies $f>f_{PWM}$ facilitates the temperature estimation of large power PMSMs, where relative values of R_S are very low, making the voltage drop $R_S i_S$ undetectable at lower frequencies.

On-line acquisition and analysis of $i_S(t)$ response to PWM excitation results in the current spectrum $I_S(j\omega)$ and allows for $Z_{IN}(j\omega) = U_S(j\omega)/I_S(j\omega)$ calculation. Under assumptions that led to Fig. 1, the active part of the input impedance $R_{IN}(\omega) = \mathrm{Re}(Z_{IN}(j\omega))$ is equal to $R_S(\omega)$. The value of R_S depends on the winding temperature θ_W, but it also changes with frequency ω. Hence, θ_W estimation has to be based on comparing $R_{IN}(\omega)$ to the value obtained at the same frequency and with a known winding temperature. In order to improve the accuracy, $R_{IN}(\omega)$ should be tracked within a range of excitation frequencies, wherever the voltage $U_S(j\omega)$ provides sufficient excitation.

B. Skin Effect

Considering AWG 7 wire, suitable for the sample PMSM machine with I_n = 48 Arms, typical skin effect depths and corresponding relative resistances are given in Table I for the frequency range of interest and for the wire out of the slot. Skin effect for the conductors placed in slots has been analyzed by several authors [14], [15]. It is well known that the wire of specific conductance $\sigma = 1/\rho$ that fits into a w-wide, l-long and h-deep slot has ac resistance of

$$R(\omega)=\frac{\mu_0\omega\, l}{4aw}\,\frac{\sin(2ah)+\sinh(2ah)}{\sin^2(ah)+\sinh^2(ah)}, \tag{1}$$

where $a^2 = \sigma\mu_0\omega/2$. At low frequencies where $ah << 1$,

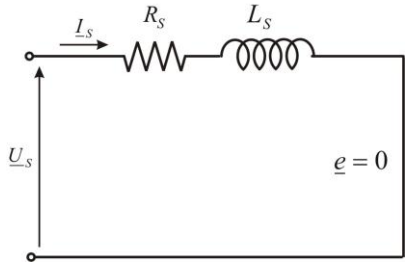

Fig. 1. High frequency equivalent circuit of an ideal PMSM.

TABLE I: Skin Effect Depth and Resistance of AWG 7 Wire

f [kHz]	0	1	10	50	100
depth [μm]	-	2000	651	291	206
$R_{relative}$	1	1.01	1.64	3.35	4.61

$$R(\omega)\approx R(0)\left(1+\frac{1}{45}\mu_0\sigma^2\omega^2h^4\right), \tag{2}$$

while at elevated frequencies, where $ah >> 1$,

$$R(\omega)\approx\frac{l}{w}\sqrt{\frac{\mu_0\omega}{2\sigma}}. \tag{3}$$

Both for low frequencies where $ah<<1$ and for elevated frequencies where $1<<ah$, the temperature affects the conductance $\sigma = 1/\rho$ and changes the resistance. Expression (2) can be reduced to $R(\omega) \approx k_1\sigma + k_2(\omega,h)\sigma^3$. Therefore, the temperature calculation at low frequencies may get involved and requires the knowledge of the slot geometry. On the other hand, (3) becomes $R(\omega) \approx k_3(\omega)/\mathrm{sqrt}(\sigma)$. Namely, high frequency resistance is proportional to $\rho^{0.5}$ for any slot geometry, which makes the temperature calculations straightforward and geometry-independent. In order to facilitate the temperature estimation and simplify the implementation, it is beneficial to consider $R(\omega)$ values obtained for a range of frequencies where $1<<ah$. For the actual machine, $ah(f_{PWM}) > 5$. Therefore, the frequency range of interest may begin with f_{PWM} and sweep through higher harmonics of the PWM pulse train.

C. Parasitic Capacitance

In order to determine the accuracy of the temperature estimator based on $R_S(\omega)$ analysis, it is necessary to study the secondary and parasitic effects. At elevated excitation frequencies, parasitic capacitance and eddy current losses in iron and permanent magnets may affect the value of $R_{IN}(\omega) = \mathrm{Re}(Z_{IN}(j\omega))$. High frequency equivalent circuits of the motor [8], [16] comprise the features that model the losses in iron and magnets, as well as the winding capacitances. For $f >$ 100 kHz, parasitic capacitances cannot be neglected [8], and the equivalent circuit has to consider distributed capacitances of the stator winding. This makes the temperature induced changes in $Z_{IN}(j\omega)$ quite involved and inadequate for the temperature estimation purposes. Therefore, the range of excitation frequencies should be $f_{PWM} < f <$ 100 kHz.

D. Eddy Current Losses

High frequency excitation produces a certain amount of losses in iron and permanent magnets. These may affect the

value of $R_{IN}(\omega)$ and impair the temperature estimation based on $R_S(\omega)$ changes. In Fig. 2 [16], the power $P_{Fe\gamma} = \omega^2 \Psi_{\gamma S}^2 / R_{Fe\gamma}$ across the resistance $R_{Fe\gamma}$ corresponds to eddy current losses in iron along the path of the flux $\Psi_{\gamma S}$. Similarly, R_{Fem} represents the losses along the main flux path, while parameters $R_{\gamma PM}$ and $L_{\gamma PM}$ represent the eddy currents and losses in permanent magnets.

Each of the eddy current losses represented by $R_{Fe\gamma}$, R_{Fem} and $R_{\gamma PM}$ in Fig. 2 increases the value of the input resistance R_{IN}. Eddy current losses modelled by $R_{Fe\gamma}$ result in an increase by $\Delta R_{Fe\gamma}$, where

$$\Delta R_{Fe\gamma} = \frac{R_{Fe\gamma} L_{\gamma S} \omega}{\left(R_{Fe\gamma}\right)^2 + \left(L_{\gamma S}\omega\right)^2}, \tag{4}$$

In the same way, the losses modelled by R_{Fem} and $R_{\gamma PM}$ in Fig. 2 increase the input resistance by ΔR_{Fem} and $\Delta R_{\gamma PM}$. Eventually,

$$R_{IN} = R_S + \Delta R_{Fe\gamma} + \Delta R_{Fe\gamma} + \Delta R_{Fe\gamma} = R_S + \sum \Delta R. \tag{5}$$

Hence, detected R_{IN} comprises temperature sensitive R_S, and it is enhanced by $\Sigma\Delta R$, which comes as the consequence of iron and magnet losses. If the value of $\Sigma\Delta R$ had the same temperature coefficient as R_S, the R_{IN}-based temperature estimation would be error-free. The output would correspond to an average temperature of the windings, iron core and magnets. As discussed next, however, the value of $\Sigma\Delta R$ decreases with temperature and impairs the precision of the temperature estimation.

Specific resistances and their temperature coefficients are given in Table II for the relevant materials. Copper and iron exhibit a similar, positive change in specific resistances. Yet, while the copper losses and $R_S(\omega)$ increase with temperature, the eddy current losses in iron are proportional to the iron conductivity $\sigma_{Fe} = 1/\rho_{Fe}$ and they decrease with temperature. Therefore, the increase $\Sigma\Delta R$ of the input resistance R_{IN}, caused by the eddy current losses decreases as the temperature rises.

The same conclusion can be drawn from (5), which expresses the impact of the losses modelled by $R_{Fe\gamma}$. The temperature rise results in an increase of the resistance $R_{Fe\gamma}$. With $L_{\gamma S}\omega << R_{Fe\gamma}$, (5) reduces to $\Delta R_{Fe\gamma} \approx L_{\gamma S}\omega / R_{Fe\gamma}$. Eventually, the consequential increase $\Delta R_{Fe\gamma}$ of the input resistance R_{IN} does decrease with temperature. The same holds true for ΔR_{Fem} and $\Delta R_{\gamma PM}$. Hence, the contribution $\Sigma\Delta R$ of eddy currents to the input resistance may impair the temperature estimation precision. For this reason, the operation of the temperature estimator has to be focused on the frequency range where $\Sigma\Delta R << R_S$.

Low frequency eddy current losses in iron and magnets may affect the value of R_{IN} to a great extent. The iron losses in a PWM supplied machine with f_{PWM} = 2 kHz are increased by 10% due to non-sinusoidal supply [17]. For the sake of comparison, it is assumed that PMSM under the test is supplied from a PWM inverter with f_{PWM} = 2 kHz. The following discussion compares the copper losses and eddy current losses at 2 kHz in order to compare the corresponding values of $\Sigma\Delta R$ and R_S.

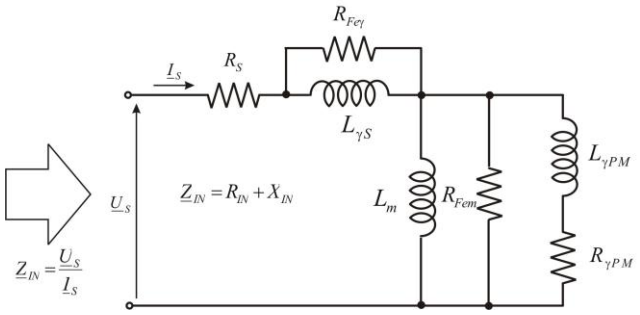

Fig. 2. High frequency equivalent circuit with main flux iron losses, leakage flux iron losses, and with losses caused by eddy currents in permanent magnets.

TABLE II: SPECIFIC RESISTANCES OF RELEVANT MATERIALS.

Material	Al	Cu	Fe	Neodym.	Sm_2Co_{17}	$SmCo_5$
ρ [Ωm] $\times 10^{-8}$	2.65	1.72	9.71	110	86	5
$\Delta\rho/\Delta T$ [1/°C] $\times 10^{-3}$	3.8	4.29	6.41	0.2	-	-

The rated iron losses of the considered PMSM reach 4% of the rated power. Therefore, the iron losses at the switching frequency of 2 kHz are, roughly, 0.4% of the rated power. For the same PMSM and the same switching frequency, the copper losses caused by the PWM current ripple reach approximately $3 \cdot R_S(f_{PWM}) \cdot \Delta I^2(f_{PWM}) \approx$ 2.4% of the rated power. Apparently, at the excitation frequency of 2 kHz, the value of $\Sigma\Delta R$ reaches 16% of R_S, thus contributing to significant estimated temperature errors.

Maintaining the amplitude of the pulsed voltage excitation at constant value, the iron losses tend to decrease [16], [17], [18] with an increase in the excitation frequency. As the frequency exceeds f_{PWM} = 10 kHz, the penetration depth of the pulsating field into the iron sheets drops below the lamination thickness, and the eddy currents in iron remain only in close vicinity of the magnetic circuit surface [16]. The total eddy current losses decrease with the penetration depth [19], and this contributes to reduction of the ratio $\Sigma\Delta R/R_S$ at elevated frequencies. Moreover, relative permeability of steel laminations reduces at higher frequencies [18], dropping to 1/2 of the initial value at 20 kHz and to 1/3 at 100 kHz. This drop in permeability μ drives the pulsating flux away from laminations and further reduces the losses.

The same conclusions can be arrived at by applying regression analysis to the loss curves of typical laminates, and approximating the iron losses at elevated frequencies by the following function:

$$p_{Fe} = \frac{\Delta P_{Fe}}{\Delta V} \approx k_k f^{1.43} B^{1.86} = k_k \left(f \cdot B\right)^{1.86} \frac{1}{f^{0.43}}. \tag{6}$$

The product $B \cdot f$ is proportional to the amplitude of the voltage excitation. With constant voltage and variable frequency excitation, the losses decrease with frequency, $p_{Fe} \sim 1/f^{0.43}$. With that in mind, at frequencies of 2 kHz, 20 kHz and 100 kHz, the ratio $\Sigma\Delta R/R_S$ assumes values of 16%, 6% and 3%, respectively. Based upon previous considerations, it is possible to determine the temperature error of $R_S(\omega)$-based temperature estimator caused by eddy currents in iron and in magnets. In cases where $R_{IN}(\omega)$ is calculated for the

frequency range [10 kHz ... 100 kHz], where the temperature changes from 25 °C up to 125 °C, and with iron and copper properties given in Table I, the temperature estimation error does not exceed 5 °C.

The values of $R_S(\omega)$ in larger PMSMs are expected to exhibit a more significant increase at higher frequencies due to skin effect being more pronounced with larger geometries. At the same time, the temperature error depends on the ratio $\Sigma\Delta R/R_S$. Therefore, the temperature estimator is bound to be more precise with larger PMSMs, of rating higher than the one used here (4.5 kW).

It is of interest to notice that the error due to the eddy currents in iron and magnets can be eliminated by calibrating the measurement system for each motor geometry. This possibility is however not considered in this paper.

E. Summary

As discussed in previous sub-sections, temperature estimation of PMSM can be based on deriving the active part of the input impedance $R_{IN}(\omega)$ over an optimal frequency range [10 kHz ... 100 kHz]. At lower frequencies, precision would be impaired by the eddy current losses in iron and in magnets, while at higher frequencies the estimator would fail due to parasitic capacitances.

III. Proposed Temperature Estimator

Temperature estimator developed in this paper makes the use of inherent PWM excitation, calculates the machine's input impedance $\underline{Z}_{IN}$, and tracks the changes of the winding temperature based on R_{IN} =Re($\underline{Z}_{IN}$) over the frequency range of [10 kHz ... 100 kHz], where both the winding capacitances and eddy current losses in magnetic circuit have just a minor impact on $R_{IN}(\omega)$, resulting in $R_{IN}(\omega) \approx R_S(\omega)$. At elevated frequencies, the values of $R_S(\omega)$ are affected by the skin effect and result in $R_S i_S$ voltage drops that are easily detectable even with a very large PMSM.

A sample spectrum of line voltages is given in Fig. 3. Fundamental (base) component is denoted by (A), it has an amplitude of 112 V, and it is out of the range shown in the Figure. Harmonic component (B) corresponds to the PWM frequency, while the component (C) coincides with $2f_{\mathrm{PWM}}$ = 10 kHz. The component (C) has twice the PWM frequency (10 kHz) and amplitude that goes well above the component (B), which has the PWM frequency (5 kHz). This is common for symmetrical space vector PWM with large modulation indices. Notice in Fig. 3 that several components in frequency band from 10 kHz up to 100 kHz exceed 10 V. These components can be used as well as an inherent excitation that aids temperature estimation.

The line voltage spectrum changes in the regime of overmodulation. In order to check the possibility to use the PWM waveform of the line voltage as an intrinsic excitation, the spectral energy has been calculated for the modulation indices that go beyond 1, up to the six-step mode, where the PWM ceases altogether, resulting in line voltages of rectangular shape. The results are summarized in Table III. They indicate that the proposed approach can be used even in overmodulation regime, as long as the operation does not enter the pure six-step mode.

TABLE III: Relative Voltage Spectrum Energy Over the Frequency Range from 10 kHz to 100 kHz in the Overmodulation Region.

Modulation index	0.9	1	1.1	1.2	1.5	six-step
10-100 kHz energy	1	0.88	0.78	0.73	0.62	0.25

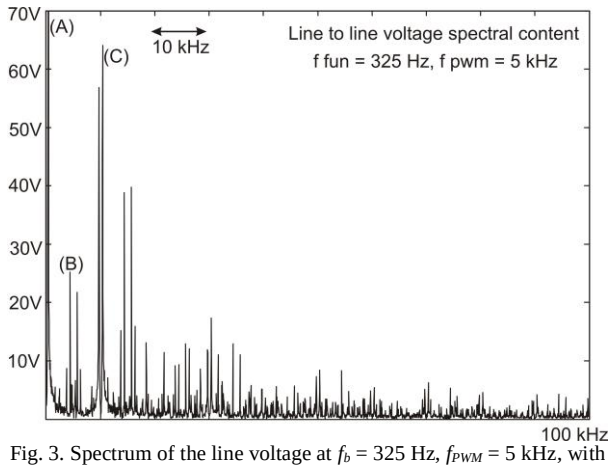

Fig. 3. Spectrum of the line voltage at f_b = 325 Hz, f_{PWM} = 5 kHz, with modulation index of 90%; frequency in [kHz] on x-axis and line voltage spectrum on y-axis.

The most important steps of the proposed method are:

- On-line spectrum analysis of the stator voltages and currents focuses on $f \in$ [10 .. 100] kHz;
- All the spectral components of the stator voltages with an amplitude well above the measurement and quantization noise are identified;
- The machine impedance $\underline{Z}_{IN}$ at given frequencies is calculated and $R_{IN}(f)$ is obtained;
- The winding temperature is calculated based upon thermal drift of the curve $R_{IN}(f)$.

On-line spectral analysis is not a problem for contemporary DSP controllers equipped with automated and DMA-driven ADC peripheral, relatively large internal RAM supporting FFT processing of large vectors, and fast CPU units capable of 150 or 300 MFLOPS.

Analysis of the stator voltages and currents for the purposes of temperature estimation does not have to be continual. Taking into account relatively slow change in machine temperatures, the voltage and current vectors can be collected and analyzed each 50 ms – 100 ms. DSP based FFT routines are mostly written in assembly language and manually optimized, as they need to make the most out of the Harvard architecture MAC cycles, which allow parallel processes and accelerate the spectrum analysis. FFT routines take successive samples of the stator voltages and currents ($u(nT)$, $i(nT)$) and produce vectors $\underline{U}$ and $\underline{I}$ with complex numbers, the amplitude and argument of which correspond to the amplitude and phase of individual spectral components. DSP based FFT routines result in discrete spectrum. As it is well known, adjacent frequency components in $\underline{U}$ and $\underline{I}$ are spaced by $\Delta f = 1/(NT)$, where $N = 2^M$ is the number of samples in time domain while T is the sampling interval. The maximum detectable frequency is $f_{max} = 1/(2T)$.

In order to cover desired frequency range, allow for a certain margin and avoid use of windowing, T is set to 1 μs.

With M = 14, the vectors of sampled data are 16 kWords long, and they cover the time span of $NT \approx 16$ ms. Hence, with M = 14 and T = 1 μs, resolution in frequency domain is Δf = 61 Hz, while the maximum detectable frequency is f_{max} = 1/(2T) = 500 kHz.

Complex numbers $\underline{U}_k$ and $\underline{I}_k$ that represent k-th frequency component of the stator voltages and currents are given with

$$\underline{U}_k = \sum_{n=0}^{N-1}\left[u(nT)\cdot\exp\left(-2\pi\,\mathrm{j}\frac{k}{N}n\right)\right], \qquad \underline{I}_k = \sum_{n=0}^{N-1}\left[i(nT)\cdot\exp\left(-2\pi\,\mathrm{j}\frac{k}{N}n\right)\right] \tag{7}$$

They make part of the vectors $\underline{U}$ and $\underline{I}$ and they represent the excitation and the machine response (current) at the frequency of k/(NT). A series of $\underline{U}_k$ and $\underline{I}_k$ values make the vectors $\underline{U}$ and $\underline{I}$ that represent the voltage and current spectrum. For each frequency $f = k/(NT)$ it is possible to calculate the machine input impedance $\underline{Z}_k$ and the equivalent input resistance using

$$\underline{Z}_k = \frac{\underline{U}_k}{\underline{I}_k}, \quad R_k = \mathrm{Re}(\underline{Z}_k), \tag{8}$$

$$\left[\underline{Z}_{163}\ \underline{Z}_{164}\ \ldots\ \underline{Z}_{1639}\right] = \underline{Z}_{IN}.$$

For k = 163...1639, the vector $\underline{Z}_{IN}$ comprises the impedance change from f = 10 kHz to f = 100 kHz. The processing of sampled voltages and currents is organized as follows:

- Samples of the phase currents and voltages are passed through the Clarke's three-phase to two-phase transformation to obtain the samples of $i_\alpha(nT)$, $i_\beta(nT)$, $u_\alpha(nT)$, and $u_\beta(nT)$.
- Four calls of FFT routine are effectuated to obtain $\underline{U}_\alpha$, $\underline{U}_\beta$, $\underline{I}_\alpha$ and $\underline{I}_\beta$.
- The motor input impedance is calculated for both α–axis and β-axis, resulting in $\underline{Z}_\alpha$ and $\underline{Z}_\beta$.
- The values of $\underline{Z}_\alpha$ and $\underline{Z}_\beta$ are used to obtain $\underline{Z}_{IN} = (\underline{Z}_\alpha + \underline{Z}_\beta)/2$, used in further processing.

Equivalent resistance R_S of the winding depends on the frequency due to skin effect [14], [15]. At the same time, temperature changes affect the specific conductivity σ of copper conductors. It is demonstrated in Section II that the winding resistance at elevated frequencies changes with the square root of the conductance σ over the whole frequency range of interest. Hence, $R(f)$ is proportional to square root of the copper specific resistance $\rho = 1/\sigma$. For a hypothetical dc excitation and a temperature rise from 0 °C up to 100 °C, the winding resistance R_{dc} would increase 1.42 times. On the other hand, for the excitation frequencies f > 10 kHz, $R(f)$ would increase only 1.19 times. Thus it follows that the proposed usage of inherent PWM excitation has a shortcoming of having a lower $\Delta R/\Delta\theta$ sensitivity.

According to (8), any frequency component within 10 kHz < f < 100 kHz range provides the possibility of finding the respective R_k, and, hence, calculating the winding temperature. It is of interest to extract reliable results, to avoid frequency components unrelated to the resistance thermal change, such as the slot harmonics, and to take into account only those results with respective amplitudes decisively above the quantization noise.

Due to a discrete number of slots and a finite number of permanent magnet modules, electromotive forces in the winding may include higher harmonics that give rise to corresponding components of the stator currents. It is of interest to exclude the results of R_k that are associated with such harmonics. At the same time, measurement noise and quantization contribute as well to spectrum components that impair the temperature estimate. As a design rule, it is adopted to emphasize R_k values obtained at frequencies where the line voltage spectrum contains a considerable excitation. In this way, slot harmonics can be suppressed by rejecting the R_k values obtained with insufficient excitation. An *average* value R_{EQ} is found over the frequency range from $K_{MIN}\Delta f$ = 10 kHz up to $K_{MAX}\Delta f$ = 100 kHz by using the weighted average. The weighted sum in nominator uses the absolute value $|\underline{U}_k|$ of the voltage excitation as the weighting coefficient:

$$R_{EQ} = \frac{\sum_{k=K_{MIN}}^{k=K_{MAX}}\left(|\underline{U}_k|\cdot R_k\right)}{\sum_{k=K_{MIN}}^{k=K_{MAX}}|\underline{U}_k|} \tag{9}$$

The value of R_{EQ} will be used as the means of estimating the winding temperature.

IV. Experimental Results

A. General Considerations

Sample PMSM under the test is a 6-pole 4.5 kW synchronous traction motor with permanent magnet excitation, wound for the line voltage of 80 Vrms and for the rated speed of n_n = 6500 rpm. Machine parameters are given in the Appendix. The motor is supplied from a three-phase PWM inverter with E_{DC} = 126 V battery, running at f_{PWM} = 5 kHz. The stator currents are obtained from Hall effect sensors that make part of the traction drive and have the rise time of 500 ns and the bandwidth of 150 kHz. The stator voltages are measured directly, by means of resistive dividers and differential amplifiers.

The temperature of the stator winding is monitored by means of three NTC sensors placed against the slot walls, as shown in Fig. 4. Stator voltage and current waveforms are given in Fig. 5 and Fig. 6, acquired at n = 6500 rpm and with the load torque of T_m = 4.7 Nm. Maintaining the speed and load, further measurements were performed for the winding temperatures of 12 °C, 33 °C, 48 °C, 69 °C, 95 °C, 101 °C, and 109 °C. For each test, the winding temperature is calculated as an average of NTC reading prior to the test and after the test.

For each initial temperature, the samples of the stator voltages and currents are collected by four-channel storage oscilloscope and processed to obtain the input impedance $\underline{Z}_k = \underline{Z}_{IN}(k\,\Delta f)$ and to derive temperature dependent resistance $R_k = R_{IN}(k\,\Delta f)$. Spectrum calculations and temperature estimation were performed off-line, on a personal computer, without involving the drive DSP controller. The vectors

comprising voltage and current samples were trimmed to 2^{14} = 16384 points, in order to be kept within the available RAM space of a typical motor controller. The scope resolution of b = 9 bits is boosted up to $b \approx 11$ bits by applying the over-sampling algorithm. The measurement interval NT was set to 26ms. The scope sampling time was T_S = 200 ns, which results in an effective T = 1.6 μs after the oversampling procedure. Adjacent frequency components in $\underline{U}$ and $\underline{I}$ are displaced by Δf =38 Hz, while the maximum detectable frequency is $f_{max} = 1/(2T) = 312$ kHz.

B. Visualizing $R_k(f)$ Data

In order to visualize and evaluate results, the frequency range from 0 up to 100 kHz is divided in 20 frequency bands, each of them 5 kHz wide. Expression (9) is used to calculate the weighted average value of R_k within each 5 kHz band. For this purpose, the values K_{MIN} and K_{MAX} in (9) are adjusted to set the lower and upper frequency limit for the given band. The outcome of this calculation consists in 20 values of R_{EQ}, each of them representing the weighted average of the winding resistance R_k within the relevant 5 kHz bands. According to (9), the average values of R_{EQ} are mainly affected by the values of R_k found at frequencies where the voltage excitation U_k is larger. Obtained in the prescribed manner, sets of 20 R_{EQ} values are shown in Fig. 7 for three different winding temperatures. Discreet values are connected by fitted curves.

Notice in Fig. 7 that the frequency change of the winding resistance deviates from the square root law anticipated in (3). While the square root law of $R(f)$ can be recognized in Fig. 7 below 60 kHz, resistance values above 70 kHz exhibit significant oscillations around the square root median. Oscillations in $R(f)$ for $f > 70$ kHz coincide with a drop of the excitation voltage U_k, which can be inferred from the spectrum in Fig. 3. They also depend on the line voltage spectrum, which gets affected by the modulation index and the fundamental frequency. At the same time, the curves on the right-hand side of Fig. 7 approach the frequencies where the winding parasitic capacitances get emphasized. The frequency change of the resistance is similar for all the three considered temperatures.

Although the curves in Fig. 7 depart from the square root change in their rightmost part, they do reflect the temperature change all over the frequency range of interest [10..100 kHz].

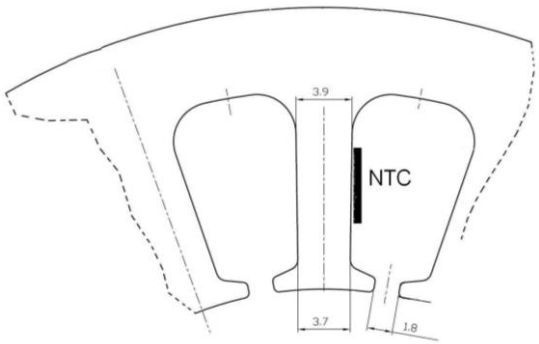

Fig. 4. Cross-section of the stator magnetic circuit with location of NTC sensors.

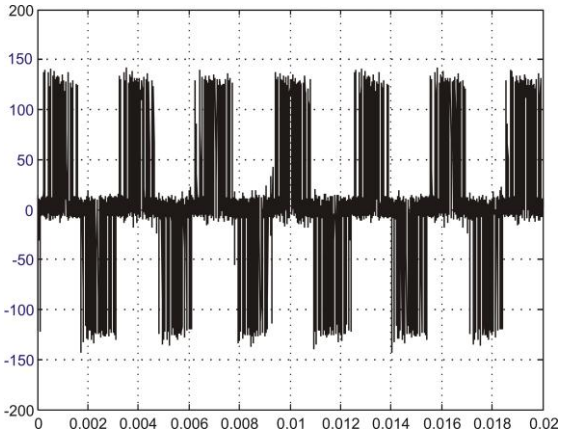

Fig. 5. Line voltage at f_b = 325 Hz, f_{PWM} = 5 kHz, with modulation index of 90%. Time is on x-axis with the scale of 2 ms/div while the line voltage is on y-axis with the scale of 50 V/div.

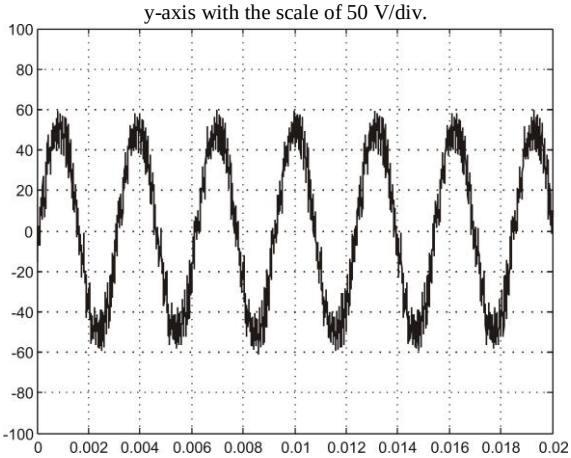

Fig. 6. Stator current at f_b = 325 Hz, f_{PWM} = 5 kHz, with modulation index of 90%. Time is on x-axis with the scale of 2 ms/div while the stator current is on y-axis with the scale of 20 A/div.

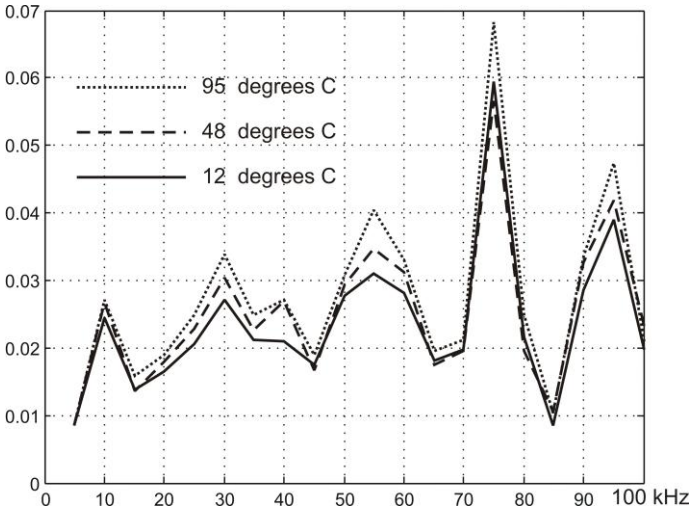

Fig. 7. Values of $R_k(f)$ for different winding temperatures. Excitation frequency in [kHz] is on x-axis. Twenty discreet values of R_{EQ} are plotted against y-axis in [Ω], each of them obtained from $R_k(f)$ within 5 kHz wide frequency bands by applying (9).

C. Temperature Estimation

The $R(f)$ curves in Fig. 7 reflect the changes in the winding temperature. The impact of the temperature change on $R(f)$

curves is consistent from 10 kHz up to 100 kHz. Therefore, the expression in (9) is applied with K_{MIN} and K_{MAX} set so as to derive the weighted average R_{EQ} now for the complete frequency range [10..100 kHz]. According to the previous consideration and (3), the value of R_{EQ} changes with the square root of the copper specific resistance. Provided that an initial value R_{EQ0}, obtained at a known winding temperature, is available, the value of R_{EQ} at any temperature and R_{EQ0} can be used to calculate the winding temperature. Within the experimental setup, the initial value is obtained as $R_{EQ0}=R_{EQ}(12\ °C)$.

In Table IV, temperature estimates are summarized for a total of 7 test events. In each test, relevant data regarding $R_k(f)$ change are weighted-averaged over the entire frequency interval from 10 kHz up to 100 kHz by using (9). For each winding temperature θ_w, (9) provides the weighted average resistance $R_{EQ}(\theta_w)$ for the given temperature.

The value of $R_{EQ0} = R_{EQ}(12\ °C)$ is obtained by repeating the same procedure five times and it is considered to be accurate. In Table IV, the value $R_{EQ}(12\ °C)$ is taken as the reference for the remaining six measurement. Hence, for the test events 2-7, the temperature estimate θ_w for the copper conductors is calculated as

$$\theta_w\left[{}^oC\right]=(235+12)\left(\frac{R_{EQ}(\theta_w)}{R_{EQ}(12^oC)}\right)^2-235 \qquad (10)$$

TABLE IV: WINDING TEMPERATURE θ_w ESTIMATES CALCULATED BY WEIGHTED-AVERAGING $R_k(f)$ OVER THE FREQUENCY RANGE FROM 10 kHz TO 100 kHz

Test No.	1	2	3	4	5	6	7
Measured θ_w [°C]	12	33	48	69	95	101	109
Estimated θ_w [°C]	-	29	43	72	96	105	111
Error in θ_w [°C]	-	-4	-5	+3	+1	+4	+2

V. DISCUSSION

Proposed method for temperature estimation is based on temperature-related changes in the input resistance R_{IN} at frequencies ranging from f_{PWM} up to, roughly, 100 kHz. The accurate value of the input resistance at PWM frequencies is difficult to obtain. Moreover, the weighted average $R_{EQ}(\theta_w)$, obtained at the given temperature θ_w depends on a number of factors, such as the cross-section of the stator conductors, the shape of the slots, machine geometry and a number of physical properties of conductors, iron sheets and permanent magnets. Therefore, the value $R_{EQ}(\theta_w)$ on its own can hardly be used to calculate the temperature θ_w, unless some prior measurements have been taken for a known temperature. Potential use of the proposed method can be organized as follows:

- Measurement of $R_{EQ}(\theta_{w1})$ is performed for a known temperature θ_{w1}. In some cases, it is reasonable to assume that the windings remain at the ambient temperature during the test, provided that the test runs immediately after the first power-up.
- The value of $R_{EQ0}=R_{EQ}(\theta_{w1})$ is taken as a reference. The actual temperature can be estimated from R_{EQ0} and from newly calculated $R_{EQ}(\theta_{w2})$ by using in essence (10),

$$\theta_{w2}\left[{}^oC\right]=(235+\theta_{w1})\left(\frac{R_{EQ}(\theta_{w2})}{R_{EQ}(\theta_{w1})}\right)^2-235 \qquad (11)$$

For all practical purposes, proposed method can be advantageously used as a means to determine the relative temperature, that is, the temperature difference with respect to a known temperature with known value of R_{EQ}, determined during the initial self-tuning of the drive, performed at a known temperature.

Validity of the temperature estimation method expressed by (9)-(11) relies on the fact that the main part of the high frequency input impedance of the machine R_{IN} is due to the skin effect in the windings. Resistance associated to this phenomenon increases with the winding temperature. On the other hand, eddy current losses in permanent magnets and in iron decrease with the temperature and impair the above conclusions. Hence, the machines with highly conductive magnets, with very large iron losses, and the machines with tiny stator conductors (where the skin effect is not pronounced) are not suitable for the application of the proposed method.

The estimated temperature corresponds to the average temperature of the whole stator winding. Hence, to identify the temperature of a specific machine part, such as the stator core or the rotor average temperature, it is necessary to include the thermal model of the machine and use the estimated temperature as an input to the thermal model calculations. In other words, proposed temperature estimator does not provide an explicit indication of the cause for the temperature rise. It may be possible to consider the slope of the estimated temperature and distinguish between faults, large instantaneous overloads and prolonged overloads, but these possibilities were not investigated in this paper. Therefore, proposed temperature estimator brings the benefit to the motor only in the above ways. The authors expect the proposed temperature estimator to eliminate the need to install temperature sensors into the stator winding, such as NTC and PTC devices frequently used in all servo motors and also in medium and large power electrical machines.

It has to be noted that the proposed method relies on detecting the high frequency currents. Therefore, the current sensors must have the bandwidth that passes the frequencies up to 100 kHz unaffected.

VI. CONCLUSION

This paper develops a novel, non-invasive method for accurate temperature estimation of inverter-fed PMSM drives. The temperature estimate is calculated from temperature related changes in the machine input impedance at elevated frequencies. The input resistance R_{IN} is detected over the frequency range from 10 kHz up to 100 kHz. It changes as the square root of the resistivity, providing the means to track the winding temperature. The PWM noise contained in the stator voltages is used as an inherent test

signal and is applied for the impedance identification. Proposed method operates without temperature sensors and without the need to inject test signal.

The temperature estimate is obtained by applying the proposed numerical algorithm to readily available signals of stator voltages and currents. For an unknown electrical machine, it is necessary to perform the first measurement at a known temperature. Further on, the temperature can be calculated from on-line measurements of stator voltages and currents, without any additional knowledge of the machine geometry, parameters, thermal equivalent circuit or other properties.

Relying on $R_S(\omega)$ values at elevated frequencies, greatly enlarged by the skin effect, makes the proposed method applicable even with large-power PMSM drives, where the voltage drop $R_S i_S$ is extremely low at fundamental frequencies.

Experimental results are obtained from a permanent magnet synchronous traction motor drive with relatively large stator conductors (I_n = 48 Arms), wherein the proposed method is used to estimate the temperature of the stator windings.

There are indications to believe that the present form of the proposed method may encounter problems in certain applications. They include permanent magnet machines with highly conductive magnets, and very low power and high voltage PMSMs which have a very small cross section of the stator conductors and negligible skin effect up to f = 100 kHz. Further work is in progress, focused on proposing a viable way to calibrate the proposed temperature estimator in cases where the skin effect is very low while eddy current losses are very high.

APPENDIX: SET-UP DATA

Permanent magnet synchronous motor

Rated power	P_n = 4.5 kW
Rated speed	n_n = 6500 rpm
Rated line voltage	U_n = 80 Vrms
Rated current	I_n = 48 Arms
Rated torque	T_n = 6.6 Nm
Number of poles	$2p$ = 6
Number of slots	Z = 18
Number of slots per pole and phase	N_{PP} = 1
Stack length	L = 131 mm
Permanent magnets	Neodymium
Stator winding: wire cross section	S_{Cu} = 8.86 mm^2
Stator winding: conductors per slot	N_{ST} = 4
Terminal-to-terminal resistance	$2R_S$ = 17.2 mΩ
Terminal-to-terminal inductance	L_{TT} = 127 μH, $L_d \approx L_q$

Three-phase PWM inverter

Dc bus voltage	E_{DC} = 126 V
Rated current	I_n = 100 Arms
PWM frequency	f_{PWM} = 5 kHz

REFERENCES

[1] R. C. Gleichman, "Failure modes and field testing of medium-voltage motor windings," *IEEE Trans. Ind. Appl.*, vol. 38, no. 5, pp. 1473-1476, Sep.-Oct. 2002.

[2] M. Ganchev, C. Kral, and T. Wolbank, "Identification of sensorless rotor temperature estimation technique for Permanent Magnet Synchronous Motor," in *Proc. Int. Symp. Power Electr., El. Drives, Autom. and Motion SPEEDAM*, pp. 38-43, 2012.

[3] S. F. Farag, R. G. Bartheld, and T. Habetler, "An integrated on-line motor protection system," *IEEE Trans. Ind. Appl.*, vol. 2, no. 2, pp. 21-26, Mar/Apr. 1996.

[4] B. Nahid-Mobarakeh, F. Meibody-Tabar, and F.-M. Sargos, "Mechanical sensorless control of PMSM with online estimation of stator resistance," *IEEE Trans. Ind. Appl.*, vol. 40, no. 2, pp. 457-471, Mar/Apr. 2004.

[5] S. D. Wilson, P. Stewart, and B. P. Taylor, "Methods of resistance estimation in permanent magnet synchronous motors for real-time thermal management," *IEEE Trans. Energy Conver.*, vol. 25 , no. 3, pp. 698-707, Sep. 2010.

[6] S. B. Lee, T. G. Habetler, R. G. Harley, and D. J. Gritter, "An evaluation of model-based stator resistance estimation for induction motor stator winding temperature monitoring," *IEEE Trans. Energy Conver.*, vol. 17, no. 1, pp. 7-15, Mar. 2002.

[7] F. Briz, M. W. Degner, J. M. Guerrero, and A. B. Diez, "Temperature estimation in inverter fed machines using high frequency carrier signal injection," *IEEE Trans. Ind. Appl.*, vol. 44, no. 3, pp. 799–808, May/Jun. 2008.

[8] S. Mahdavi and K. Hameyer, "High frequency equivalent circuit model of the stator winding in electrical machines," in *Proc. 10th Int. Conf. Elect. Machines ICEM*, pp. 1706-1711, 2012.

[9] Y. Hua, M. Sumner, G. Asher, Q. Gao, and K. Saleh, "Improved sensorless control of a permanent magnet machine using fundamental pulse width modulation excitation," *IET Elec. Power Appl.*, vol. 5, no. 4, pp. 359-370, Apr. 2011.

[10] Q. Gao, Y. Hua, M. Sumner, and G. Asher, "Comparison of two sensorless permanent magnet synchronous motor drives fed by a matrix converter and a voltage source inverter using fundamental PWM excitation signals," in *Proc. 13th Euro. Conf. Power Electron. and Appl. EPE*, Barcelona, Spain, CD-ROM, 2009.

[11] Y. Hua, M. Sumner, G. M. Asher, and Q. Gao, "Sensorless control for a PM machine with reduced current distortion using space vector PWM excitation," in *Proc. 13th Euro. Conf. Power Electron. and Appl. EPE*, Barcelona, Spain, CD-ROM, 2009.

[12] Q. Gao, G. M. Asher, and M. Sumner, "Zero speed position estimation of a matrix converter fed AC PM machine using PWM excitation," *13th Int. Power Electron. and Motion Control Conf.*, Poznan, Poland, pp. 2261-2268, Sep. 2008.

[13] Q. Gao, G. M. Asher, M. Sumner, and P. Makys, "Position estimation of ac machines over a wide frequency range based on space vector PWM excitation," *IEEE Trans. Ind. Appl.*, vol. 43, no. 4, pp. 1001-1011, July/Aug. 2007.

[14] O. M. O. Gatous and J. Pissolato, "Frequency-dependent skin-effect formulation for resistance and internal inductance of a solid cylindrical conductor," *Proc. IEE Microw., Antennas and Propag.*, vol. 151, no. 3, pp. 212–216, Jun. 2004.

[15] O. M. O. Gatous and J. Pissolato Filho, "A new formulation for skin-effect resistance and internal inductance frequency-dependent of a solid cylindrical conductor," in *Proc. IEEE/PES Transm. & Dist. Conf. - Latin America*, pp. 919-924, 2004.

[16] G. R. Slemon and M. L. Awad, "On equivalent circuit modeling for synchronous machines," *IEEE Trans. Energy Conver.*, vol. 14, no.4, pp. 982-988, Dec. 1999.

[17] A. Boglietti, A. Cavagnino, and M. Lazzari, "Fast method for the iron loss prediction in inverter-fed induction motors," *IEEE Trans. Ind. Appl.*, vol. 46, no. 2, pp. 806-811, Mar/Apr. 2010.

[18] N. Bowler, "Frequency-dependence of relative permeability in steel," *Review of Quantitative Nondestructive Evaluation*, vol. 25, ed. by D. O. Thompson and D. E. Chimenti, CP820, American Institute of Physics, pp. 1269-1276, 2006.

[19] A. E. Emanuel, "The effect of nonsinusoidal excitation on eddy current losses in saturated iron," *IEEE Trans. Power Del.*, vol. 3, no. 2, pp. 662-671, Apr. 1988.

Nikola Z. Popov was born in Belgrade, Serbia. He received B.Sc. (2008) and M.Sc. (2010) in Electrical Engineering from the University of Belgrade. Since 2010 he has been with the Faculty of Electrical Engineering, University of Belgrade, where he is currently a research and teaching assistant in the Department of Power Engineering and Power Drives. His main areas of research are electrical machines parameter estimation, design and control of power converters and variable-speed drives.

Slobodan N. Vukosavic (M'93, SM'12) was born in Sarajevo, Yugoslavia, in 1962. He received the B.S., M.S., and Ph.D. degrees from the University of Belgrade, Belgrade, Yugoslavia, in 1985, 1987, and 1989, respectively, all in Electrical Engineering. He was with the Nikola Tesla Institute, Belgrade, Yugoslavia, until 1988, when he joined the ESCD Laboratory of Emerson Electric, St. Louis, MO. Since 1991, he has been a consultant with Vickers Electric Company/MOOG Electric. He is currently Professor at the University of Belgrade. His interests include digital control, power conversion in renewable energy sources and power quality. He has published over 70 papers, 3 textbooks and 7 monographs and has completed over 40 large R/D and industrial projects.

Emil Levi (S'89, M'92, SM'99, F'09) received his M.Sc. and PhD degrees from the University of Belgrade, Yugoslavia in 1986 and 1990, respectively. From 1982 till 1992 he was with the Dept. of Elec. Engineering, University of Novi Sad. He joined Liverpool John Moores University, UK in May 1992 and is since September 2000 Professor of Electric Machines and Drives. He serves as Co-Editor-in-Chief of the IEEE Trans. on Industrial Electronics, as an Editor of the IEEE Trans. on Energy Conversion, and as Editor-in-Chief of the IET Electric Power Applications. Emil is the recipient of the Cyril Veinott award of the IEEE Power and Energy Society for 2009.